Journal of Hydraulic Research

ISSN: 0022-1686 (Print) 1814-2079 (Online) Journal homepage: https://www.tandfonline.com/loi/tjhr20

Application of weakly compressible and truly incompressible SPH to 3-D water collapse in waterworks

Eun-Sug Lee, Damien Violeau, Réza Issa & Stéphane Ploix

To cite this article: Eun-Sug Lee, Damien Violeau, Réza Issa & Stéphane Ploix (2010) Application of weakly compressible and truly incompressible SPH to 3-D water collapse in waterworks, Journal of Hydraulic Research, 48:sup1, 50-60, DOI: 10.1080/00221686.2010.9641245

To link to this article: https://doi.org/10.1080/00221686.2010.9641245

Published online: 03 Dec 2010.

Journal of Hydraulic Research Vol. 48 Extra Issue (2010), pp. 50–60
doi:10.3826/jhr.2010.0003

Application of weakly compressible and truly incompressible SPH to 3-D water collapse in waterworks

Application de SPH faiblement compressible et vraiment incompressible à l'écrasement 3D de l'eau sur des ouvrages hydrauliques

EUN-SUG LEE, *Saint-Venant Laboratory for Hydraulics, Université Paris-Est, Joint Research Unit EDF R&D, CETMEF, Ecole des Ponts, 6 quai Watier, 78400 Chatou, France*

DAMIEN VIOLEAU, *Saint-Venant Laboratory for Hydraulics, Université Paris-Est, Joint Research Unit EDF R&D, CETMEF, Ecole des Ponts, 6 quai Watier, 78400 Chatou, France. E-mail: damien.violeau@edf.fr (author for correspondence)*

RÉZA ISSA, *Saint-Venant Laboratory for Hydraulics, Université Paris-Est, Joint Research Unit EDF R&D, CETMEF, Ecole des Ponts, 6 quai Watier, 78400 Chatou, France*

STÉPHANE PLOIX, *EDF R&D, Clamart Cedex - 1 avenue du Général de Gaulle, 92141, France*

ABSTRACT
Two algorithms of the SPH Lagrangian numerical method, the first weakly compressible, the second truly incompressible, are presented and applied to two free-surface three-dimensional flows. The first (schematic) case consists of a water column collapsing in a rectangular tank with a central rectangular obstacle, and allows the comparison and validation of both algorithms. It appears that the incompressible method is superior to predict the total strength experienced by the obstacle, while the weakly compressible method shows weaknesses under this criterion. The second application case, very close to an industrial study, represents a "ski-jump" spillway connecting the reservoir of a river dam to a valley with complex bottom shape. The global flow pattern is compared to laboratory observations from a physical model, leading to satisfactory conclusions which prove SPH has the potential to be a promising method for the design of complex waterworks.

RÉSUMÉ
Deux algorithmes de la méthode numérique lagrangienne SPH, l'un quasi-incompressible, l'autre rigoureusement incompressible, sont présentés et appliqués à deux cas d'écoulements à surface libre tridimensionnels. Le premier cas, schématique, représente l'effondrement d'une colonne d'eau dans un bassin parallélépipédique avec un obstacle central, et permet la comparaison et la validation des deux algorithmes. Il met en évidence la supériorité de la méthode incompressible pour le calcul des efforts exercés sur l'obstacle, tandis que la méthode quasi-incompressible se révèle très insuffisante de ce point de vue. Le second cas d'application, très proche d'une étude industrielle, consiste en un évacuateur de crue de type "saut de ski" déversant le contenu d'un réservoir de barrage dans une vallée de forme complexe. L'allure globale de l'écoulement est comparée avec les observations d'un modéle physique, aboutissant à des conclusions prometteuses quant à l'emploi futur de la méthode SPH pour l'aide au dimensionnement d'ouvrages d'eau complexes.

Keywords: Dam-break, Lagrangian methods, numerical modelling, reservoir, spillway, SPH

1 Introduction

Smoothed Particle Hydrodynamics (SPH) is now widely used for research applications on free-surface flows (see e.g. Dalrymple and Rogers 2006), but still few industrial cases have been treated (according to publications), mainly for practical reasons based on the computational cost of this method, especially in three dimensions. However, recent work in parallelism for SPH (e.g. Rogers *et al.* 2007, Moulinec *et al.* 2008, Ferrari *et al.* 2009) now allows simulations of flows under real conditions near river or coastal waterworks, such as waves breaking on a sea defense or an offshore work, as well as flows in fish-passages (Violeau *et al.* 2008) and dam spillways. In section 2, we present two SPH algorithms (weakly compressible and truly incompressible, respectively) and apply them in section 3 to problems of 3-D water collapse, starting with a schematic case for validation before going up to the case of a dam spillway based on an existing configuration. Our purpose is to show the feasibility of SPH for "real-life" applications.

Revision received December 1, 2009/Open for discussion until June 30, 2010.

2 Numerical model

2.1 *Weakly compressible SPH*

We solve the Navier-Stokes equations for weakly compressible or incompressible flows. The weakly compressible form of these equations is assumed to be

$$\frac{d\mathbf{u}}{dt} = -\frac{1}{\rho}\nabla p + \nu\Delta\mathbf{u} + \mathbf{g} \tag{1}$$

$$\frac{d\rho}{dt} = -\rho\nabla\cdot\mathbf{u} \tag{2}$$

$$p = \frac{\rho_0 c_0}{\gamma}\left[\left(\frac{\rho}{\rho_0}\right)^{\gamma} - 1\right] \tag{3}$$

where $\mathbf{u}$ is the velocity vector, while ρ and p denote the fluid density and pressure, respectively. All of them are field variables, while the other quantities appearing in (1) to (3) are constants, namely the gravity vector $\mathbf{g}$, the speed of sound c_0, the reference density ρ_0, the molecular kinetic viscosity ν and the exponent of Tait's state equation $\gamma = 7$. We thus neglect the effects of compressibility in the viscous terms of the momentum equation (1), as well as turbulent effects, since our applications will be dominated by gravity, pressure and advection (see section 3). We also neglect surface tension, since we work at very large scales. However, all these neglected effects can be easily accounted for in the coming SPH algorithm when it is proved to be necessary (see e.g. Violeau and Issa (2007) for turbulence; see Hu and Adams (2007) for surface tension). The first two equations of the system, (1) and (2), are solved in time through a first-order explicit scheme, while (3) doesn't require any scheme:

$$\frac{\mathbf{u}^{(n+1)} - \mathbf{u}^{(n)}}{\delta t} = -\frac{1}{\rho^{(n)}}[\nabla p]^{(n)} + \nu[\Delta\mathbf{u}]^{(n)} + \mathbf{g} \tag{4}$$

$$\frac{\rho^{(n+1)} - \rho^{(n)}}{\delta t} = -\rho^{(n)}[\nabla\cdot\mathbf{u}]^{(n)} \tag{5}$$

$$\rho^{(n+1)} = \frac{\rho_0 c_0}{\gamma}\left[\left(\frac{\rho^{(n+1)}}{\rho_0}\right)^{\gamma} - 1\right] \tag{6}$$

where the superscripts (n) refer to the iteration number and δt is a time step defined in section 2.3. The fluid is now discretised in particles; using the basic SPH interpolants to write the spatial derivatives in a Lagrangian discrete form (see e.g. the recent review by Monaghan 2005), we obtain a system of explicit equations giving the velocity vector, the density and the pressure of each particle at time $n+1$ as a function of the same quantities at time n:

$$\begin{aligned}(\mathbf{u})_a^{(n+1)} = \mathbf{u}_a^{(n)} &+ \delta t\mathbf{g} \\ &- \delta t\sum_b m_b\left(\frac{p_a^{(n)}}{[p_a^2]^{(n)}} + \frac{p_b^{(n)}}{[p_b^2]^{(n)}}\right. \\ &\left. - \frac{16\nu}{\rho_a^{(n)} + \rho_b^{(n)}}\frac{\mathbf{u}_{ab}^{(n)}\cdot\mathbf{e}_{ab}^{(n)}}{[r_{ab}^2]^{(n)} + \eta^2}\right) w_{ab}^{\prime(n)}\mathbf{e}_{ab}^{(n)}\end{aligned} \tag{7}$$

$$\rho_a^{(n+1)} = \rho_a^{(n)} + \delta t\sum_b m_b\mathbf{u}_{ab}^{(n)}\cdot w_{ab}^{\prime(n)}\mathbf{e}_{ab}^{(n)} \tag{8}$$

$$\rho_a^{(n+1)} = \frac{\rho_0 c_0}{\gamma}\left[\left(\frac{\rho_a^{(n+1)}}{\rho_0}\right)^{\gamma} - 1\right] \tag{9}$$

where the subscripts a and b refer to particles, e.g. $\mathbf{u}_a^{(n)}$ is the velocity of particle a at time n, and η is a small parameter used to avoid singularities. With our notations, $w'_{ab}\mathbf{e}_{ab}$ stands for $\nabla_a w_{ab}$ in most of the SPH papers available in the literature. Here we call $\mathbf{r}_a$ the position vector of particle a and m_a its mass, and we use the following notations:

$$\mathbf{u}_{ab} = \mathbf{u}_a - \mathbf{u}_b \tag{10}$$

$$\mathbf{r}_{ab} = \mathbf{r}_a - \mathbf{r}_b \tag{11}$$

$$r_{ab} = |\mathbf{r}_{ab}| \tag{12}$$

$$\mathbf{e}_{ab} = \frac{\mathbf{r}_{ab}}{r_{ab}} \tag{13}$$

$$w'_{ab} = w'_h(r_{ab}) \tag{14}$$

where w'_h is the derivative of the spatial (isotropic) kernel used to quantify particle interactions. As usual in SPH, we define a constant smoothing length h and write the kernel in a dimensionless form, i.e. $w'_h = f'(q = r/h)$. In the following, we use several kernels; we present below the fourth-order spline kernel whose derivative is defined by

$$f'(q) = -\frac{1}{5\pi h^4}\begin{cases}\left(\frac{5}{2}-q\right)^3 - 5\left(\frac{3}{2}-q\right)^3 + 10\left(\frac{1}{2}-q\right)^3 & \\ \qquad\qquad\qquad\qquad \text{if } 0 \le q \le 0.5 & \\ \left(\frac{5}{2}-q\right)^3 - 5\left(\frac{3}{2}-q\right)^3 \quad \text{if } 0.5 \le q \le 1.5 & \\ \left(\frac{5}{2}-q\right)^3 \qquad\qquad \text{if } 1.5 \le q \le 2.5 & \\ 0 \qquad\qquad\qquad\qquad \text{if } 2.5 \le q\end{cases} \tag{15}$$

When equations (7) to (9) are solved, the particle positions are updated from

$$\mathbf{r}_a^{(n+1)} = \mathbf{r}_a^{(n)} + \delta t\mathbf{u}_a^{(n+1)} \tag{16}$$

2.2 *Truly incompressible SPH*

The weakly incompressible algorithm described above (and slightly different versions) have proved for a long time to be efficient when applied to a wide range of flows including confined and free-surface flows (see e.g. Violeau and Issa 2007, Dalrymple and Rogers 2006). However, it has been noticed that this approach suffers from serious drawbacks when estimating pressure. Several methods have been developed to circumvent this; for example, MLS (Moving Least-Squares) interpolants (see Colagrossi and Landrini 2003) or Shepard filtering (see Dalrymple and Rogers 2006) or ISPH (Incompressible SPH) (see Lee *et al.* 2008). In the present work, we focus on ISPH by solving a system

of incompressible Navier-Stokes equations:

$$\frac{d\mathbf{u}}{dt} = -\frac{1}{\rho}\nabla p + \nu\Delta\mathbf{u} + \mathbf{g} \tag{17}$$

$$\nabla \cdot \mathbf{u} = 0 \tag{18}$$

By avoiding the use of any state equation, the corresponding algorithm is more accurate, but more complex since the pressure must be calculated implicitly. We thus separate the forces in two parts in order to change the time scheme to

$$\frac{\mathbf{u}^{(n+1/2)} - \mathbf{u}^{(n)}}{\delta t} = \nu\Delta\mathbf{u}^{(n)} + \mathbf{g} \tag{19}$$

$$\Delta p^{(n+1)} = \frac{\rho}{\delta t}\nabla \cdot \mathbf{u}^{(n+1/2)} \tag{20}$$

$$\frac{\mathbf{u}^{(n+1)} - \mathbf{u}^{(n+1/2)}}{\delta t} = -\frac{1}{\rho}\nabla p^{(n+1)} \tag{21}$$

instead of (4) to (6). The algorithm thus takes the form of a predictor-corrector method with an intermediate velocity field $\mathbf{u}_a^{(n+1/2)}$ resulting from the predictor step (19). Equation (20) is a Poisson equation solved to predict the pressure, which is then used to project the intermediate velocity field on a divergence-free space by applying the correction step (21). The resulting velocity $\mathbf{u}_a^{n+1}$ is thus rigorously incompressible (theoretically), i.e. it satisfies the incompressible continuity equation (18) in its SPH discrete form. A relevant SPH formulation of the latter algorithm reads

$$\mathbf{u}_a^{(n+1/2)} = \mathbf{u}_a^{(n)} + \delta t\mathbf{g} + \frac{8\nu\delta t}{\rho}\sum_b m_b \frac{\mathbf{u}_{ab}^{(n)} \cdot \mathbf{e}_{ab}^{(n)}}{[r_{ab}^2]^{(n)} + \eta^2} w_{ab}'^{(n)} \mathbf{e}_{ab}^{(n)} \tag{22}$$

$$\sum_b m_b \frac{p_{ab}^{(n+1)} r_{ab}^{(n)}}{[r_{ab}^2]^{(n)} + \eta^2} \dot{w}_{ab}^{(n)} = -\frac{\rho}{2\delta t}\sum_b m_b \mathbf{u}_{ab}^{(n+1/2)} \cdot w_{ab}'^{(n)} \mathbf{e}_{ab}^{(n)} \tag{23}$$

$$\mathbf{u}_a^{(n+1)} = \mathbf{u}_a^{(n+1/2)} - \frac{\delta t}{\rho^2}\sum_b m_b (p_a^{(n+1)} + p_b^{(n+1)}) w_{ab}'^{(n)} \mathbf{e}_{ab}^{(n)} \tag{24}$$

where the density is now considered as a constant and $p_{ab} = p_a - p_b$. Compared to the weakly compressible algorithm, the main difference lies in equation (23), which takes the form of a linear system with unknowns $p_a^{(n+1)}$. It is solved here with the Bi-CGSTAB (Bi-Conjugate Gradient STABilized) method (Van Der Vorst 1992). Although our coefficient matrix system in equation (23) is symmetric, Bi-CGSTAB is applied since it has been proved to be robust and to have smoother and faster convergence behaviour than other linear solver. The above algorithm (or similar variations) were proved to be efficient for confined and free-surface flows (see e.g. Lee *et al.* 2008, Shao 2005).

2.3 *Numerical features*

Both algorithms described above, (7) to (9) for weakly compressible SPH (WC-SPH) and (22) to (24) for its incompressible counterpart (ISPH), are constrained by the following definition of the time step (Morris *et al.* 1997):

$$\delta t = \min\left(0.4\frac{h}{U}, 0.25\sqrt{\frac{h}{F}}, 0.125\frac{h^2}{\nu}\right) \tag{25}$$

where U and F are characteristic velocity and force, respectively. For WC-SPH, U is equal to c_0, the numerical speed of sound appearing in (3), here chosen in order to keep the density fluctuations under 1%, i.e. $c_0 = 10U_{\max}$ (typically), $U_{\max}$ being the maximum flow speed (Monaghan, 1994). For ISPH, U is simply equal to $U_{\max}$, which increases the time step by a factor ten and thus significantly reduces the computational time, although the algorithm requires the resolution of the Poisson equation (23). The characteristic force F occurring in (25) is defined by

$$F = \max_a |\mathbf{F}_a^{(n)}| \tag{26}$$

where $\mathbf{F}_a^{(n)}$ is the force experienced by a particle during the predictor step, i.e. the summation appearing in the right-hand-side of (22).

Wall boundary conditions are assumed through the technique of wall particles and fictitious particles (see Violeau and Issa 2007). For ISPH, a particular treatment is applied to those fictitious particles to ensure the appropriate pressure wall condition (see Lee *et al.* 2008). The free surface does not require any particular condition in WCSPH, while pressure must be set to zero for free-surface particles in ISPH (Lee *et al.* 2008). Initial conditions consist of a set of particles localised on a Cartesian 3-D grid with constant spacement δr in all directions. The smoothing length is proportional to the latter, i.e. $h = \alpha\delta r$ with $\alpha = 1.0$ to 1.5 for the applications presented in section 3. The definition (15) thus shows that the fourth-order kernel support is of size $2.5\,\alpha\delta r$.

The finiteness of the kernel support means that only a limited number of neighbour particles b play a role in all the sums appearing in equations like (22). This is used to reduce the computational time by building a link list between particles at each time step. The symmetry of all equations with respect to particles' labels a and b is also an important feature of the proposed numerical scheme. Besides its property of conservativity (see Bonet and Lok 1999), it also helps to increase the performances of the computation by reducing the required operations and memory by a factor two. However, despite these interesting improvements, parallelism is still an important issue to carry out 3-D simulations in an industrial context. Our code (Spartacus-3D) has been parallelized through the MPI library according to the process described by Moulinec *et al.* (2008).

3 Applications to 3-D water collapse

3.1 *Water collapse in a tank*

The first application presented here is one of the test cases suggested by SPHERIC (SPH European Research Interest Community) in order to validate the SPH method. Since 3D WCSPH

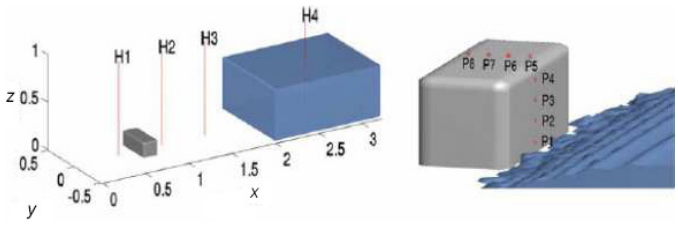

Figure 1 Geometry of the 3-D dam-break experiment (from Kleefsman *et al.* 2005) with measurement positions (unit: m). Right: Zoom of the box

was recently parallellized and 3D ISPH is a relatively new development, these two approaches are herein validated through this test case.

3.1.1 *Geometry of the system*

Based on the experimental configuration (see Kleefsman *et al.* 2005), a rectangular box is located in an open roof tank. The geometry and the measurement positions are briefly described in Fig. 1; the points H1 to H4 are used to observe the water heights (a detailed description can be found in Moulinec *et al.* 2008), while P1 to P8 are pressure sensors on the box (see Fig. 2 for the details). In the experiment, water is hold by a gate and released by pulling up the gate instantly. In the numerical study, instead of modelling the gate motion, the water is released immediately when the simulation is started.

3.1.2 *Modelling and simulation conditions*

The discretisation of the system is presented in Table 1 for WCSPH and ISPH. The initial particle distance δr is decided by locating 30 fluid particles along the initial water height (equal to 0.55 m). A wall is consisted of one layer of wall and three layers of fictitious particles. The different number of wall particles between WCSPH and ISPH is due to the limitation of ISPH being a serial code. Such a number of total particles for 3D ISPH cannot be handled by one processor in our case and this limitation with ISPH also affects the choice of the kernel and the smoothing length ratio $\alpha = h/\delta r$, leading to smaller than the one

Table 1 Fluid, wall and fictitious particle discretisations for the 3-D dam-break flow

	WCSPH	ISPH
Fluid particles	$67 \times 54 \times 30$	
Wall particles	38,142	16,079
Fictitious particles	113,592	49,101
Total particle number	260,274	173,720
Initial particle spacing: $\delta r(m)$	55/3000	

Table 2 SPH parameters for the 3-D dam-break flow

	WCSPH	ISPH
Order of the kernel	4th	3rd
Smoothing length ratio α	1.5	1.0
Reference velocity U (ms^{-1})	60	7.333

used in WCSPH (see Table 2). A spanwise direction periodicity is thus applied in ISPH by removing the x–z planes, while non-periodicity is set for WCSPH.

As explained in section 2.3, the time step in WCSPH is controlled by the smoothing length $h = 0.0275$ m and the speed of sound $U = c_0 = 60$ m/s through (25), i.e. $\delta t = 1.8333\ 10^{-4}$ s. On the other hand, the time step in ISPH is set to 10^{-3} s as in Kleefsman *et al.* (2005). With $h = 0.018333$ m, this is in accordance to (25) with a reference velocity $U = U_{\max} = 7.333$ m/s. The time step is thus 5.46 times smaller in WCSPH. A constant viscosity 10^{-6} m^{2}s^{-1} is chosen, and a zero velocity is applied for the wall particles. In ISPH, surface particles have to be tracked down to set their pressure to zero (see Lee *et al.* 2008); calculating the following quantity:

$$\nabla \cdot \mathbf{r} \simeq \frac{m_b}{\rho_b} \mathbf{r}_{ab} \cdot w'_{ab} \mathbf{e}_{ab} \tag{27}$$

This is equal to 3 for 3-D applications in the core of domain and far below this value for surface particles. In this simulation, a criterion to identify surface particles is set at 2.4.

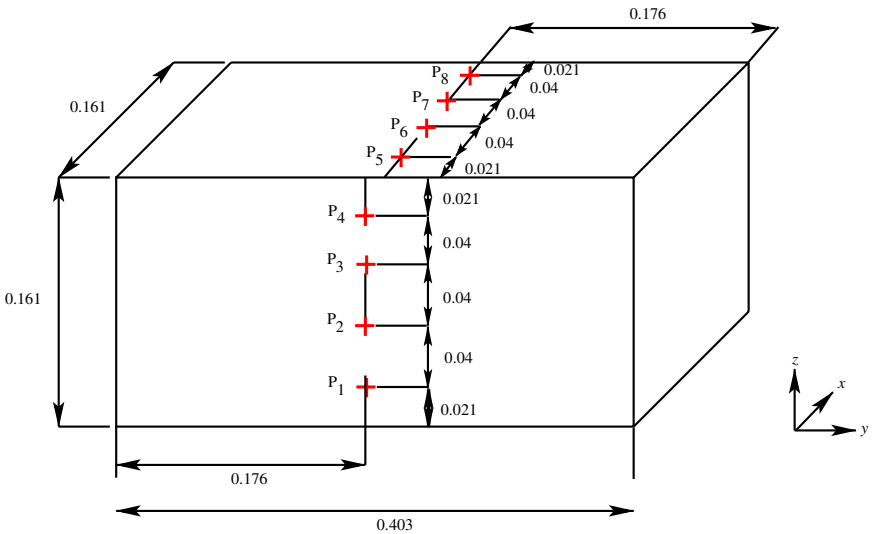

Figure 2 Measurement positions for the pressure on the box

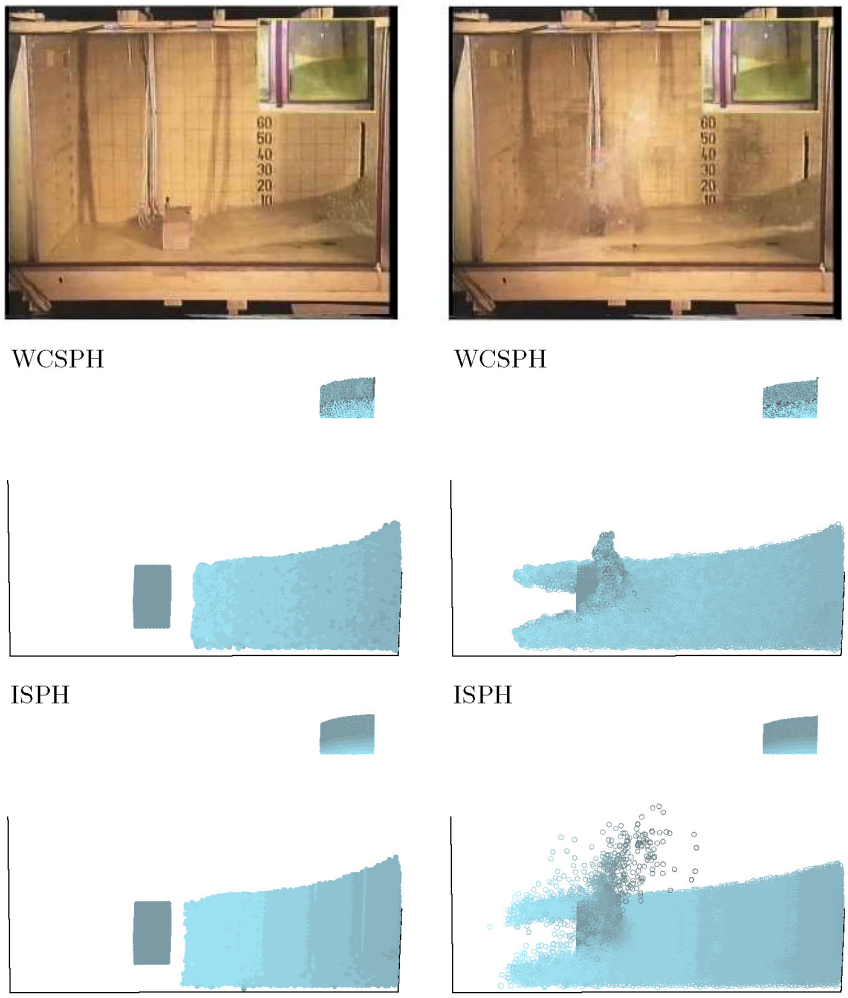

(a) Comparisons at $t = 0.4$ s (b) Comparisons at $t = 0.56$ s

Figure 3 Snapshots of the 3-D dam-break flow compared with experiment (Kleefsman *et al.* 2005), at $t = 0.4$ s and $t = 0.56$ s (note that WCSPH is at $t = 0.41$ s and $t = 0.6$ s). SPH results are in terms of velocity. the small picture are the water behind the gate and SPH results are coloured by pressure

The parallel WCSPH runs with 16 processors, each processor has 2.6 GHz CPU and 4 Gb RAM, while the serial ISPH is carried out on a processor with 3.2 GHz CPU and 2 Gb RAM.

3.1.3 *Results*

All the SPH results in this section are compared with the experiment and VOF (Volume Of Fluid) results in Kleefsman *et al.* (2005). First of all, the snapshots from the experiment and SPH methods are shown, especially the velocity field for SPH, at the physical times $t = 0.4$ s and 0.56 s (see Fig. 3). Note that the WCSPH results are presented at the slightly different physical times $t = 0.41$ s and $t = 0.60$ s. In each snapshot, the small pictures on the top right represent the water behind the gate, especially the pressure field for SPH. It shows that far smoother velocity and pressure fields are obtained with ISPH. A better prediction of the splash-up behaviour is also shown in ISPH than WCSPH when the first impact of the water occurs on the box (see Fig. 3b).

The time histories of water height at the locations H4 and H2 are depicted in Fig. 4. The global behaviours of WCSPH and ISPH are pretty much similar but slightly shifted about 0.2 s after 2.5 s at H4 (behind the gate) and 4.5 s at H2 (between the gate and the box). In the comments of their VOF simulations, Kleefsman *et al.* pointed out that an underprediction of the water speed was resulting from the use of a coarse grid, which indicates that our results could be improved by increasing the resolution, i.e. the number of fluid particles. Further study will be made on this. The predicted water surface elevation by ISPH appears to be lower than that by WCSPH and the experiment at H2 from 4.3 s and at H4 from 5 s. This is due to the penetration of a few fluid particles through the wall in ISPH while WCSPH keeps all the fluid particles in the domain. By increasing the spatial resolution in ISPH, the number of losing particles are getting smaller. Hence, the water elevation at these physical time will be better predicted. However, further work will be needed to improve the impermeability of solid wall in ISPH. The spikes in ISPH at H2 is due to the splashed water particles after hitting the box.

The pressure on the front box (P1 and P3), facing towards the water comes from behind the gate, and on the top of the box (P5 and P7) are shown in Fig. 5. As already presented in Lee

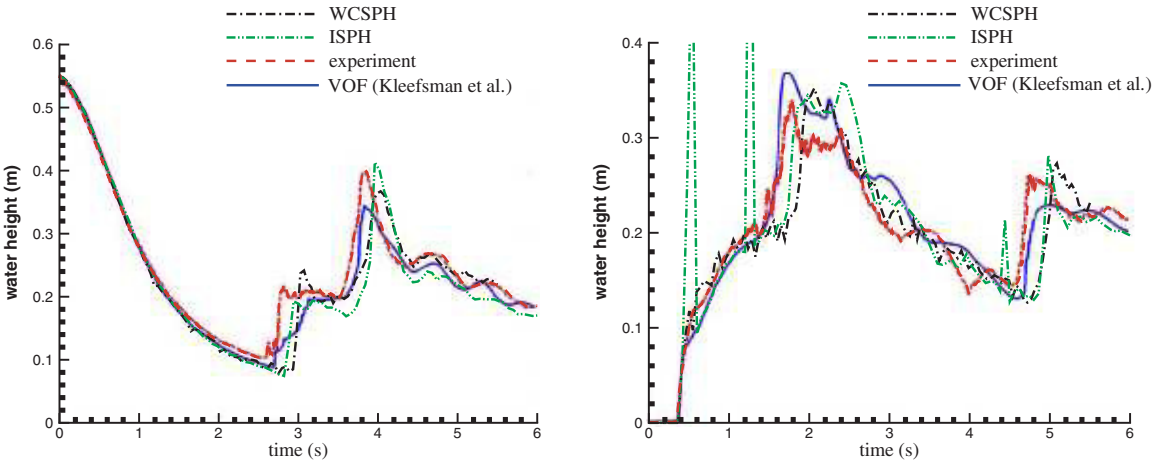

(a) SPH methods vs experiment at H4 (b) SPH methods vs experiment at H2

Figure 4 Water height time histories of the 3-D dam-break flow at H4 and H2

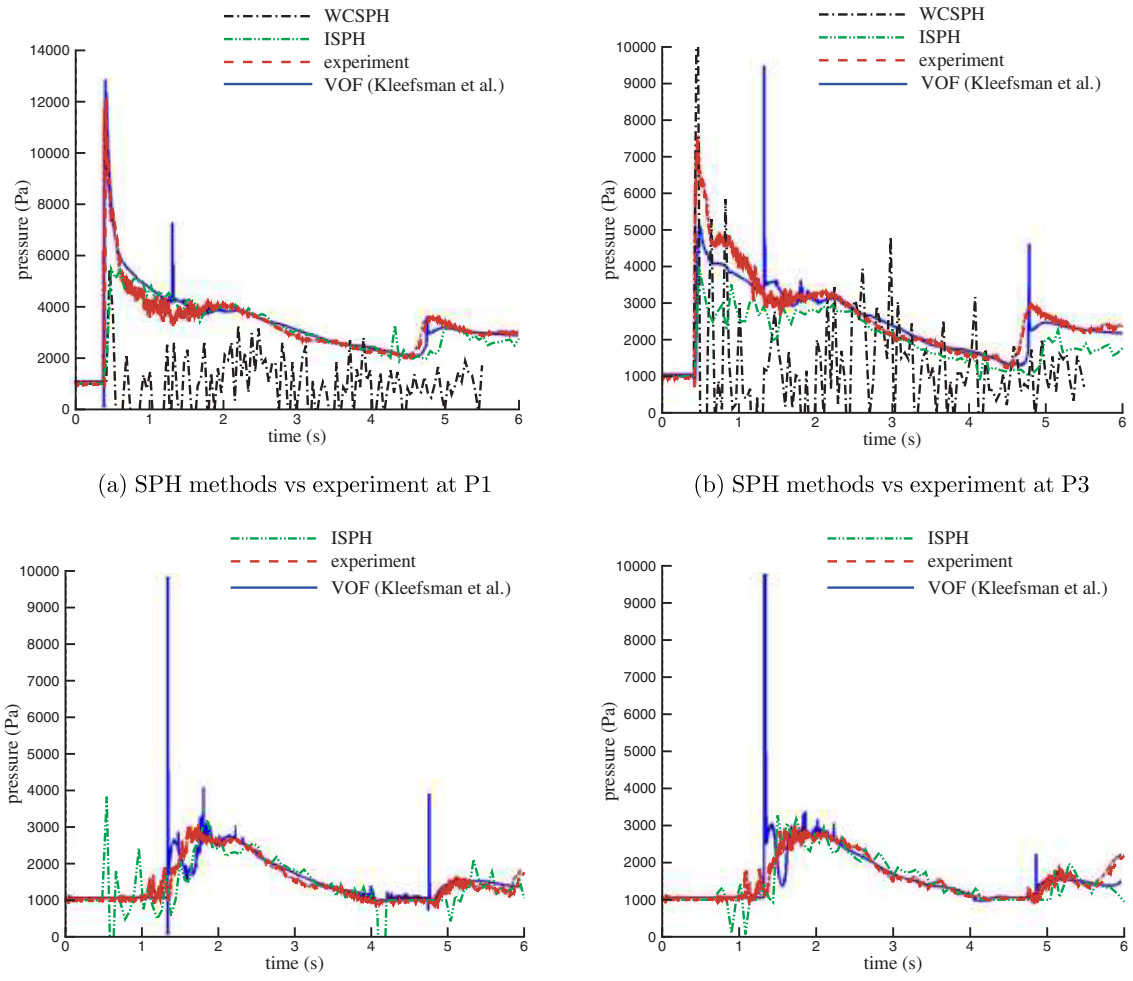

(a) SPH methods vs experiment at P1 (b) SPH methods vs experiment at P3

(c) ISPH vs experiment at P5 (d) ISPH vs experiment at P7

Figure 5 Pressure time histories of the 3-D dam-break flow at P1, P3, P5 and P7. Note that WCSPH results for P5 and P7 are not shown here due to the strong pressure fluctuation as in P1 and P3

et al. (2008), pressure from WCSPH shows strong fluctuations and this also appeared here at all the positions. Thus, only the pressure at P1 and P3 is illustrated for WCSPH. On the other hand, ISPH is smoother and shows a behaviour in accordance with the experiment, except an underestimation of the pressure during the first impact on the box. The second impact around 4.7 s is also visible in ISPH with some delay (P1 and P3). In ISPH, especially for gravity flows, hydrostatic pressure is applied as

Table 3 Comparisons of CPU time for the 3-D dam-break flow.

Methods	WCSPH	ISPH
Number of processors	16	1
Time step: δt (s)	$1.833\ 10^{-4}$	$1.0\ 10^{-3}$
Physical time: t(s)	5.5 s	6.0 s
CPU time (h)	32.0/processor	48.5

an initial condition. When the wall is far away from the fluid particles, their initial pressure condition is zero. During the first impact, the wall started to interact with the fluid but no information stems from the previous time step. The pressure at this point is thus underestimated and gradually catches up as the time goes which explaines that delay. The pressure on the top of the box (P5 and P7) shows a fairly good agreement, although some fluctuations appear, which might be due to the wall treatment based on fictitious particles (see Lee, 2007). We have tested the Shephard filter on density during the PhD work associated to Lee (2007). however, this was not as good as ISPH. Moreover, ISPH has an advantage over other methods in terms of CPU time (see Lee *et al.* 2008) since it requires larger time step than the one in WCSPH.

The CPU time needed for WCSPH and ISPH are indicated in Table 3. The different physical time between WCSPH and ISPH is due to the different time step. Each processor in WCSPH takes 32 hours for this simulation. If it ran with only one processor, the total CPU time would be 512 hours, whereas ISPH takes only 48.5 hours. The speed-up of the parallel WCSPH code is presented in Moulinec *et al.* (2008).

3.2 *River dam spillway*

Our SPH code is now applied to an industrial case, namely a real river dam spillway in three dimensions. Spillways are hydraulic structures designed in order to evacuate flood water without damaging a dam. To investigate the capacity of the spillway, an experimental and/or numerical study is necessary. Nowadays, the computer power has been increased enough to allow such studies. For such a study, parallelism is required; we thus used our WCSPH algorithm, extended to massive parallelism on IBM BlueGene/L and BlueGene/P machines. Especially, our code can handle 75 million particles on BlueGene/P. Specific tools for pre- and post-processing are also essential to generate a complex geometry and analyse the results. At this stage, the main objective of this work is thus to examine the feasibility of this type of study.

3.2.1 *Geometry of the system*

We consider the dam spillway of Goulours, in Ariége, Midi-Pyrénées (France). A physical model has been built at EDF R&D with a scale factor equal to 20 (see Fig. 6). Although this dam has two types of spillways, a ski-jump and a PK-weir (Piano-Key weir), only the ski-jump spillway is considered here for the numerical study. An overview of the whole geometry is shown in Fig. 7.

3.2.2 *Modelling and simulation conditions*

The Goulours valley was digitalized with a specific pre-processing tool. Next, the spillway and the reservoir were built from a Cartesian particle network, then combined to the geometry of the valley (see Fig. 8). For simplicity, the dam reservoir is schematically represented by a rectangular tank rather than the real geometry. The wall here consists of one layer of wall particles and only one layer of fictitious particles with a distance of $2\delta r$ from the edge. This is due to the complexity of the valley bathymetry, which also requires too much memory for 3 layers of dummy particles as in the schematic case of the previous section. The discretisation of the system is indicated in Table 4 with the numbers of particles used for the valley in parenthesis.

In terms of SPH numerical parameters, a 4th-order kernel is used with a smoothing length ratio $\alpha = 1.5$, and the numerical speed of sound c_0 is set at $600\,\mathrm{ms}^{-1}$. Again, a constant viscosity of $10^{-6}\,\mathrm{m}^2\mathrm{s}^{-1}$ is used and a zero velocity at the wall is prescribed.

3.2.3 *First results*

An example of the results from the experimental and numerical (SPH) models is presented in Fig. 9. This is only to show the motion of the water past the ski-jump, which is qualitatively correct, but more quantitative comparisons should be made before any further conclusion. In the experiment, water level on the

(a) Real dam site in Ariège, France (b) Physical model at EDF

Figure 6 The real site of Goulours dam and its physical model

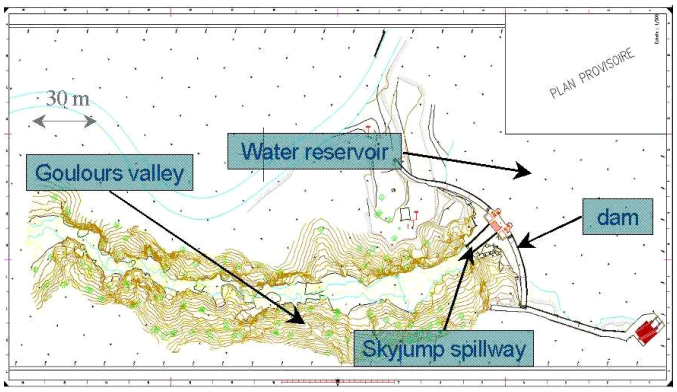

Figure 7 Geometry of the Goulours valley and the dam

spillway was measured when the flow is steady and also the location of the jet at the valley. The quantitative comparisons will be made for the next stage by adapting the precise experimental configurations. However, as a first attempt, the numerical simulation runs for 16 s of physical time without considering the

Table 4 Fluid, wall and fictitious particle discretisations for the 3-D river dam spillway. The numbers of particles used for the valley are in parenthesis

Fluid particles	500,000
Wall particles	216,967(176,025)
Fictitious particles	219,633 (176,025)
Total number of particles	936, 600
Initial particle spacing: δr (m)	0.2

experimental conditions and a time sequence of the results is presented in Fig. 10 from the top front view. All the SPH results presented in this section are visualised by the post-processing tool 'pv-meshless', which is extended from ParaView© to deal with particle based data (see Biddiscombe *et al.* 2008). This simulation takes about 5 days of CPU time with 1,024 processors on BlueGene/L. It shows that SPH can handle such 'real-life' applications in the field of free-surface flows.

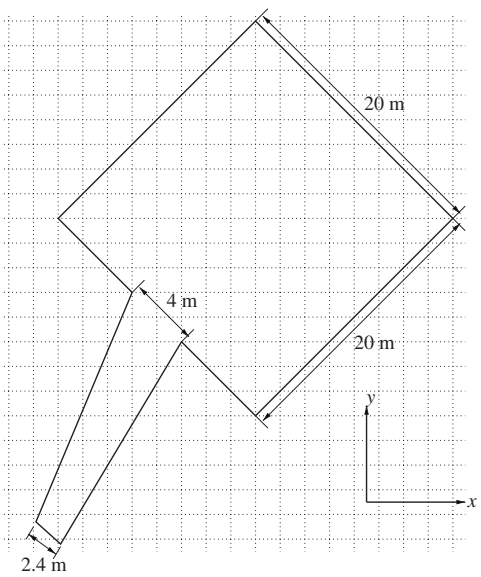

(a) Top view for reservoir and spillway

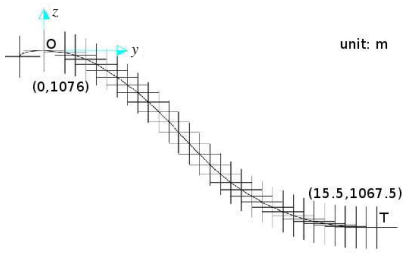

(b) The slope of the real spillway bed

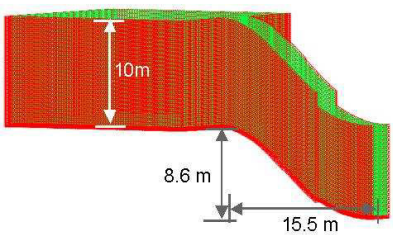

(c) Side view for reservoir and spillway

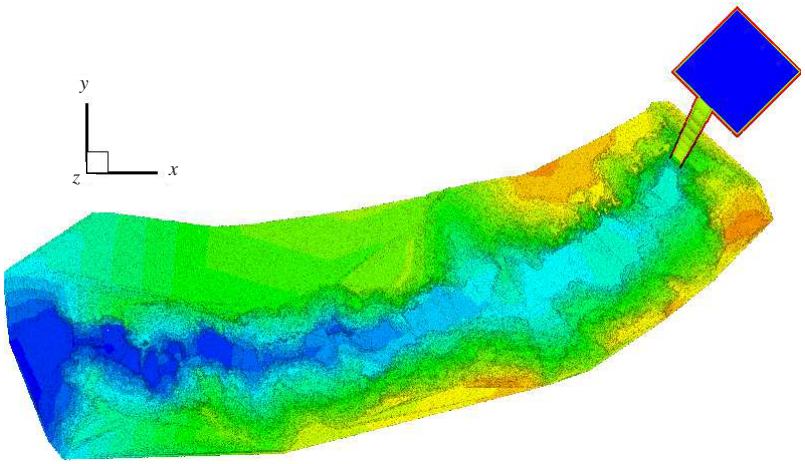

(d) Top view of the whole geometry including the valley

Figure 8 Numerical system modelling of the 3-D river dam spillway

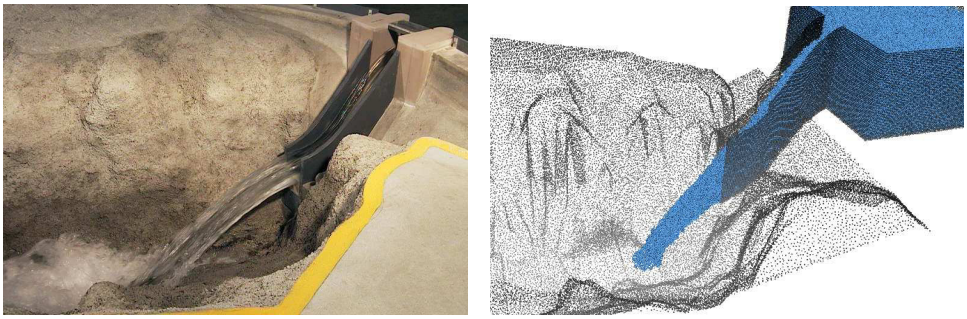

Experiment WCSPH

Figure 9 An example of the 3-D river dam spillway snapshot from the physical (left) and numerical (right) models

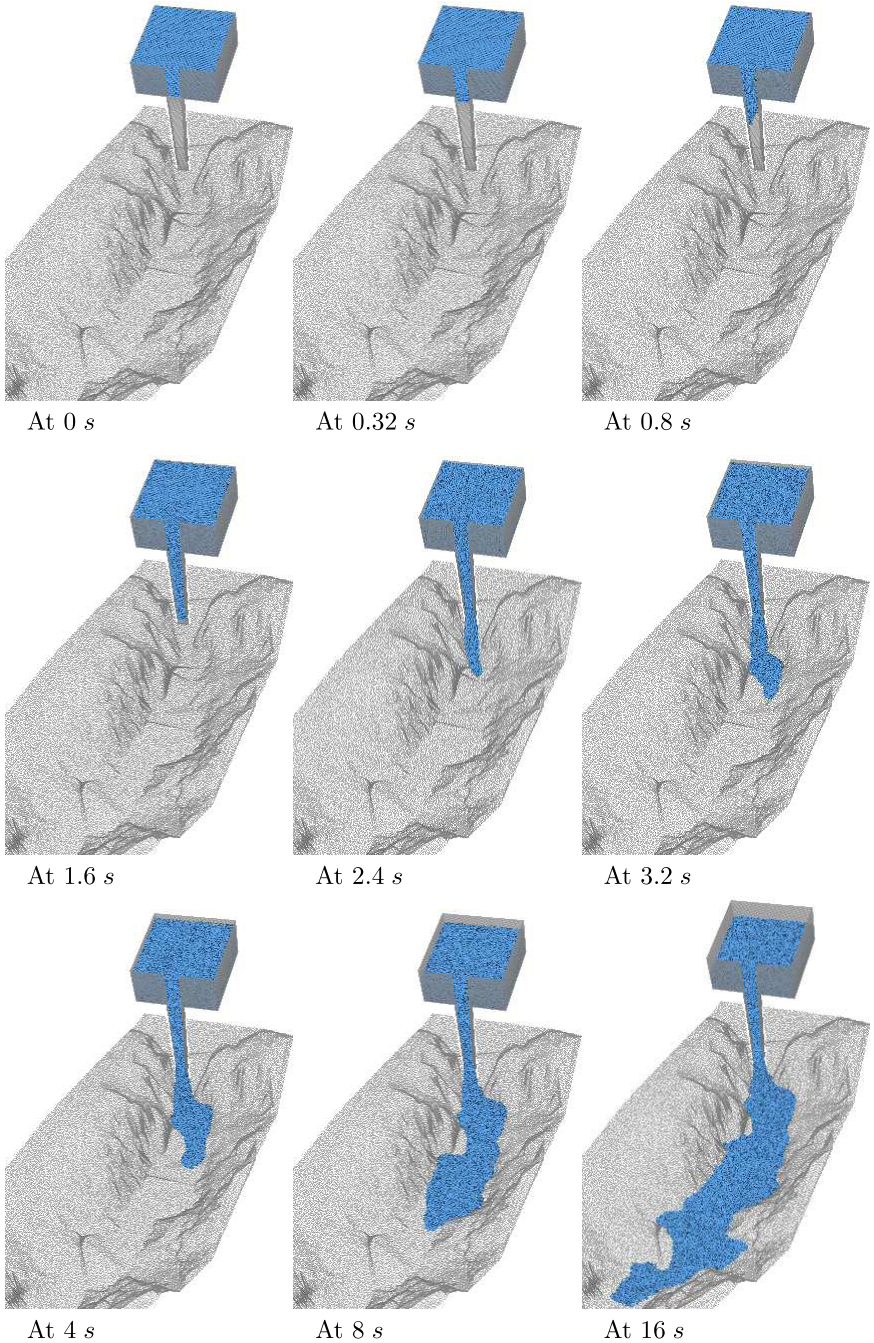

Figure 10 Time sequence of the 3-D dam spillway flow modelled with WCSPH

4 Conclusions

A parallel WCSPH (weakly compressible SPH) method and a serial ISPH (incompressible SPH) method are validated through a 3-D water collapse in a tank with an obstacle. The pressure predicted by WCSPH is not realistic, while ISPH shows satisfactory results even with a smaller kernel support. In order to get optimum results, the kernel support should be increased in ISPH, thus requiring parallelizing this algorithm too. Relatively small pressure oscillations appear, which might be due to the wall boundary condition. Improving wall boundary treatment is an important issue in SPH for hydraulics. Both WCSPH and ISPH shows some delay in the motion of the free surface, which might be due to the coarse particle size.

A river dam spillway also runs with massively parallelized WCSPH. The objective of this work is fulfilled by showing some qualitative results, showing the capability of SPH to handle simulations of free-surface flows with waterworks at the industrial scale. In a future stage of the present work, experimental conditions will be applied to the numerical simulations and allow quantitative comparisons between them. The latter will concern the pressure distribution on the spillway, the free-surface elevation and the discharge coefficient. Again, the prediction of pressure will require to overcome the main drawback of WCSPH, i.e. making the ISPH algorithm parallel.

Acknowledgments

Most of the work presented here were carried out within the frame of Marie Curie Transfer of Knowledge Agreement ESPHI (European SPH Initiative). The first test case with ISPH (water collapse in a tank) was carried out at The University of Manchester funded by EPSRC (Grant GR/S28310).

Notation

c_0 = Numerical speed of sound
e = Unit vector between particles
f' = Derivative of dimensionless kernel
$\mathbf{F}$ = Force vector
F = Characteristic force
$\mathbf{g}$ = Gravity acceleration
h = Smoothing length
m = Mass
n = Iteration number
p = Pressure
$\mathbf{r}$ = Position vector
r = Norm of $\mathbf{r}$
$\mathbf{u}$ = Velocity vector
U = Characteristic velocity
$U_{\max}$ = Maximum velocity
w'_h = Derivative of kernel
α = Smoothing length factor ($= h/\delta r$)
γ = Exponent of the state equation
δr = Initial particle distance
δt = Time step
η = Correction factor
ν = Molecular kinematic viscosity
ρ = Density
ρ_0 = Reference density

Subscripts and superscripts
a = Particle
b = Neighbouring particle
ab = Particle difference ($A_{ab} = A_a - A_b$)
(n) = Value at iteration n

References

Biddiscombe, J., Graham, D., Maruzewski, P., Issa, R. (2008). *Visualization and analysis of SPH data*, Ercoftac Bulletin.

Bonet, J., Lok, T.-S.L. (1999). Variational and momentum preservation aspects of Smoothed Particle Hydrodynamics formulations. *Comput. Meth. Appl. Mech. Eng.* 180, 97–115.

Colagrossi, A., Landrini, M. (2003). Numerical simulation of interfacial flows by Smoothed Particle Hydrodynamics. *J. Comput. Phys.* 191(2), 448–475.

Dalrymple, R.A., Rogers, B.D. (2006). Numerical modelling of water waves with the SPH method. *Coastal Engng.* 53, 141–147.

Fawer, C. (1937). Etude de quelques ecoulements permanents a filets courbes. Thesis, Universite de Lausanne. La Concorde, Lausanne, Switzerland [in French].

Ferrari, A., Dumbser M., Toro, E.F., Armanini, A. (2009). A new 3D parallel SPH scheme for free surface flows. *Computers & Fluids* 38, 1203–1217.

Hu, X.Y., Adams, N.A. (2007). An incompressible multi-phase SPH method. *J. Comput. Phys.* 227, 264–278.

Kleefsman, K.M.T., Fekken, G., Veldman, A.E.P., Iwanowski, B., Buchner, B. (2008). A Volume-of-Fluid based simulation method for wave impact problems. *J. Comput. Phys.* 206, 363–393.

Lee, E.-S. (2007). Truly incompressible approach for computing incompressible flow in SPH and comparisons with the traditional weakly compressible approach, *PhD thesis*.

Lee, E.-S., Moulinec, C., Xu, R., Violeau, D., Laurence, D., Stansby, P. (2008). Comparisons of weakly compressible and truly incompressible SPH algorithms for 2D flows. *J. Comput. Phys.* 227, 8417–8436.

Monaghan, J.J. (1994). Simulating free surface flows with SPH. *J. Comput. Phys.* 110, 399–406.

Monaghan, J.J. (2005). Smoothed Particle Hydrodynamics. *Rep. Prog. Phys.* 68, 1703–1759.

Morris, J.P., Fox, P.J., Zhu, Y. (1997). Modelling low Reynolds number incompressible flows using SPH. *J. Comput. Phys.* 136, 214–226.

Moulinec, C., Issa, R., Marongiu, J.-C., Violeau, D. (2008). Parallel 3-D SPH simulations, *Comput. Model. Engng. Sci.* 25(3), 133–148.

Rogers, B., Dalrymple, R.A., Stansby, P.K., Laurence D.R.P. (2007). Development of a parallel SPH code for free-surface

wave hydrodynamics, Proc. 2nd SPHERIC International Workshop, Madrid (Spain), 23rd–25th May 2007, 111–114.

Shao, S. (2005). SPH simulation of solitary wave interaction with a curtain-type breakwater. *J. Hydr. Res.* 33(4), 366–375.

Van Der Vorst, H.A. (1992). Bi-CGSTAB: A fast a smoothly converging variant of Bi-CG for the solution of nonsymmetric linear systems. *S. J. Sc. Stat. Comput.* 13, 631–644.

Violeau, D. and Issa, R. (2007). Numerical modelling of complex turbulent free surface flows with the SPH Lagrangian method: An overview. *Intl. J. Num. Meth. Fluids* 53(2), 277–304.

Violeau, D., Issa, R., Benhamadouche, S., Saleh, K., Chorda, J., Maubourguet, M.-M. (2008). Modelling a fish passage with SPH and Eulerian codes: The influence of turbulent closure, Proc. 3rd *SPHERIC International Workshop*, 3rd–6th June 2008, Lausanne, (Switzerland)